Effect of surface texture on the adhesion performance of laser treated Ti6Al4V alloy

MARESSA, PIETRO; ANODIO, LUCA FRANCESCO; BERNASCONI, ANDREA; DEMIR, ALI GOKHAN; PREVITALI, BARBARA

Effect of Surface Texture on the Adhesion Performance of Laser Treated Ti6Al4V Alloy

PIETRO MARESSA, LUCA ANODIO, ANDREA BERNASCONI, ALI GÖKHAN DEMIR, and BARBARA PREVITALI

Department of Mechanical Engineering, Politecnico di Milano, Milan, Italy

1. INTRODUCTION

Many industrial applications demand high structural integrity while maintaining light weight, which are met by high performance alloys, like titanium. Considering the difficulty in machining and forming these alloys [1,2], assembly of different parts to generate the final component provides ease of manufacturing, reduction of scrap due, and modularity in terms of using standard semi-finished material. For assembling titanium alloys the use of fasteners such as bolts and nuts, or rivets for joints is possible. Such joints can be replaced, which provides ease of maintenance. In this case, the induced problems are related to the introduction of notches due to holes for rivets and bolts, increase in weight, and the risk of galvanic corrosion between the component and fastener materials. Another approach is based on the use of permanent joints via welding. Due to the high reactivity of titanium, welding of these alloys has to be carried out in inert atmosphere. Therefore, the key technologies for titanium alloy welding are based on the use of an electron beam in vacuum [3] or a laser beam assisted by an inert process gas such as Ar or He [4]. Another welding technique adaptable to titanium alloys is friction stir welding that does not require inert atmosphere, however it shows limitations in terms of weld and component geometries [5]. Another important aspect regarding the use of titanium alloys is that it might be required to join them to other metals or even non-metallic materials. While fasteners can be adequate to most of the material couples, welding technologies are limited to join titanium alloys with other metallic alloys, and some polymeric materials. Another option that is widely used in aeronautics and aerospace applications, which also receives an increasing attention for joining titanium alloys, is the use of adhesives [6–8]. Adhesive bonding provides flexibility in joint design and is cost effective due to the reduced machining time and scrap material. Moreover, the notch effects related to the generation of assembly holes are avoided. Joining of dissimilar materials is also possible with the adequate bond design, where the titanium alloy can be joined to polymers, ceramics, and composite materials.

Surface preparation plays a crucial role in the design of an adhesive joint. The advantages given by surface modification, especially on titanium alloys, are the increase of contact surface and formation of an oxide layer on the material that bonds to the polymer molecules of the adhesive [9]. The state of the art in surface modification of titanium to improve the bonding includes physical processes such as sand or grit blasting, chemical processes like etching, anodization, and Pasa Jell treatment (PRC-DeSoto International, Inc, Sylmar, CA, USA) as well as thermal treatments like plasma spray [10–14]. A great majority of these processes contain hazardous chemical components and heavy metals such as Cr that are also harmful to the environment. Due to stringing health and safety regulations regarding their use and disposal,

cleaner alternatives to these processes are required in the industrial practice. Surface preparation based on chemical reactions also renders the manufacturing process prone to variations. Moreover, they do not provide control over the surface microgeometry obtained by the treatment as they are of stochastic nature. The topography of the surfaces obtained by such surface treatments is commonly aggregated to surface roughness parameters. Today, an increasing attention is present toward tailored or designed surfaces, in order to fulfill the required function of a component. A greater control on the surface geometry in micrometric and even sub-micrometric dimensions becomes evidently important. Laser microprocessing with pulsed sources is a highly promising option due to flexibility of machinable surface geometries, adaptability to different component sizes and shapes, and possibility to fully integrate the surface production to a digital environment based on CAD/CAM interfaces. This process presents advantages compared to the others in terms of eco-compatibility, easy manufacturability, and repeatability.

Galantucci et al. used excimer laser treatment of metals and carbon fiber composites to improve the adhesion joint strength [15]. The authors used large laminar spot to modify the surface roughness, which they have observed to reduce glycerine contact angle (CA). On pure aluminum samples they have improved the adhesion strength by 70% compared to plain samples. On the other hand, the term of "laser surface texturing," has been used in a publication by Wong et al. in 1997 for the first time [16]. This paper showed sub-mm size dimples, realized with surface melting and evaporation by a Nd:YAG system, proposed to improve adhesion behavior, although they did not provide any results on the adhesion performance. Molitor and Young proposed the use of excimer laser to structure the titanium surfaces by large area melting and ablation [17]. They showed that the treatment significantly improved the surface wettability and adhesion properties of Ti-15-3 alloy/glass fiber reinforced epoxy composite bond. Moreover, they deduced that durability of the titanium was the weakest factor in this adhesion bond system. Later, Baburaj et al. proposed microcolumn arrays on commercially pure titanium obtained with excimer laser [18]. Their results showed threefold increase in the shear rupture strength of bonded specimens compared to non-treated ones. These authors attributed the outcome mainly to the geometrical changes such as the increase of the surface area, and generation of sub-micron sized locking sites, as well as improved wettability due to generation of titanium oxides. On the other hand Spadaro et al., used a Nd:YAG system to obtain surface textures based on remelting to increase surface area on 2024 aluminum specimens [19]. The results indicated an improvement of up to double the adhesive fracture energy compared to specimens that have been only degreased. Man et al. demonstrated the use of a fiber laser to texture titanium alloy surfaces with varying microhole densities to induce mechanical grip [20]. These authors demonstrated that a density of 100 microholes per cm^2, 125 µm in diameter, and 550 µm in depth, improved the fracture load 30% and 80%

compared to grit grinding and sand-blasting, respectively. Laser surface texturing was also used to improve adhesion of coatings and medical implants. In particular, Lamraoui et al. showed the use of laser surface texturing on Al 2017 substrates prior to thermal spray coating of a Ni–Al powder [21]. Arrays of microholes generated by a fiber laser source enabled better contact between the coating and the substrate leading to improve the interface toughness. Other authors suggested the use of microholes to improve the adhesion of titanium implants to human tissue [22,23]. More recently Alfano et al. employed low power laser ablation on aluminum and stainless steel substrates. The authors showed that laser processing on the metallic substrates improved joint strength by 100% for aluminum alloy/epoxy joints and by 25% for stainless steel/epoxy combinations, compared to substrates prepared by degreasing [24].

It can be observed that the improvement induced by the laser surface treatment is a mixed effect of increased surface area, mechanical grip, and change in surface chemistry. As a matter of fact, the laser treatment contributes to change all these aspects simultaneously. From this point of view, the effect of surface texture geometry has been investigated sparingly. Laser micromachining based on direct writing is a flexible method for conventional marking and engraving processes, and can be used to improve adhesion joint strength to generate controllable or tailored surface geometries. Moreover, the introduction and industrial diffusion of high brilliance pulsed solid state fiber and DPSS lasers in the last decade provided easier operation with robust systems, and reduced capital and maintenance costs. These factors render laser surface texturing of large components an industrially viable process.

This work presents the results of preliminary investigations on the effect of laser surface texturing on Ti6Al4V alloy and its effect on adhesive bonding performance, from the surface geometry perspective. In particular, three distinct surface patterns are conceptualized, and the laser surface texturing process is studied with a highly productive and industrial ns-pulsed Q switched fiber laser. The bonding with the use of epoxy based adhesive is explained. The adhesion strength is evaluated via shear tests on lap-joint configuration. The proposed surfaces are compared to non-textured (plain) and sand blasted surfaces. The results showed significant improvements up to sevenfold stronger bonds compared to plain surfaces. Moreover, post-rupture failure analysis is reported, which revealed potential improvements to further increase the bond strength with the proposed method.

2. EXPERIMENTAL

The experimental section covers the equipment for laser surface texturing, as well as the designed surface concepts, bonding preparation, and testing of

the bond strength. Throughout the work, Ti6Al4V alloy 8 mm thick was used. The specimens were cut in rectangular form with 114.3 mm × 25.4 mm dimensions by abrasive water jet, and were cleaned with alcohol for degreasing and removal of dirt prior to laser surface texturing.

2.1. Laser Surface Texturing Strategies

Surface texturing was realized using a Q-switched active fiber laser (YLP-1/100/50/50 from IPG Photonics, Oxford, MA, USA) with pulse duration of about 100 ns (full width at half maximum) and a wavelength of 1064 nm. Laser beam manipulation was achieved using a scanning head (TDS TSH 8310 from Sunny Technology, Beijing, China), which housed a focusing lens with a focal length of 100 mm. In this configuration the calculated beam diameter on the focal plane was 39 μm. Machining was done in ambient atmosphere without any process gas. The laser system details are given in Table 1.

In order to improve surface adhesion three different kinds of textures were designed to introduce effects that would be favorable for increasing the bond strength. In particular these effects consist of the increase of the contact surface, the realization of mechanical interlocking introducing microcavities able to retain the adhesive, and finally the realization of undercuts that are able to reduce the risk of adhesive failure since the shift of the adhesive is blocked along the direction perpendicular to the surface of the material. Since the processing was done in ambient atmosphere, changes in surface chemistry were expected due to oxidation. Three surfaces that incorporated these mentioned effects were hypothesized as surface design, namely dimpling, grid, and chaotic (Fig. 1).

The first surface design concept, namely dimpling, consisted of the commonly used microholes (Fig. 1(a)). These microholes would primarily provide increase of surface area and mechanical grip perpendicular to the shear direction. Laser surface texturing with such geometry consists of point-by-point percussion drilling operation. With adequate parameter choice by mainly using a few number of pulses, the texturing of dimpled surfaces can be highly productive. A number of pulses is sent on the material surface, while the laser beam is stationary, and then the beam is moved to the position of the next

TABLE 1 Main Characteristics of the Used Pulsed Fiber Laser Source

Laser wavelength	1064 nm
Maximum average power	50 W
Maximum pulse energy	1 mJ
Minimum pulse duration (FWHM)	100 ns
Pulse repetition rate	20–80 kHz
Beam quality factor (M^2)	1.7
Focal distance	100 mm
Focused laser beam diameter	39 μm
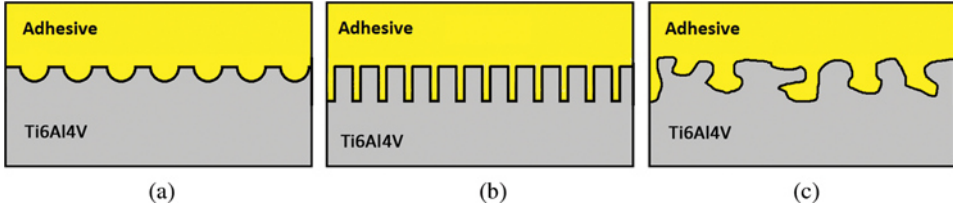
FIGURE 1 Conceptual sections of the designed adhesion surfaces: (a) dimpling, (b) grid, (c) and chaotic.

hole. It is also possible to generate all the holes on the surface and apply consecutive passes to enlarge them, which is favorable to reduce the thermal load and have a better control of the hole depth. The hole diameter is in the order of the laser beam size and together with the hole depth is determined by the laser energy (E) and the number of pulses, or the number of consecutive passes (n). On the other hand the hole pitch (p) is imposed by the user, which was set as 0.1 mm that generated a density of 10^4 holes/cm^2. The strategy employed in this work used ramped emission profiles, which used modulation duration (t_{mod}) rather than a fixed number of pulses that is explained in detail elsewhere [25]. A certain jump delay after each microhole drilling is applied to stabilize positioning of the galvanometric mirrors and laser emission (t_{delay}). The laser processing parameters for the dimpling surface texture are reported in Table 2.

The concept of the grid derives from the aim to increase the hole density on a line in both X and Y axes to a saturation level, thus they merge. The resulting surface pattern would become a grid with more area for contact and mechanical grip (Fig. 1(b)). The grid texture was realized digging perpendicular channels on the material surface, based on linear scans. The width and the depth of the cavities are determined by the laser energy (E), pulse repetition rate (PRR), scan speed (v), and number of passes (n). The machining parameters for the grid texture are reported in Table 3.

TABLE 2 Laser Micromachining Parameters for Dimpling Surface Texture. Machining Conditions are Based on Point-by-Point Percussion Drilling

Parameter		Dimpling
Modulation duration	t_{mod} (μs)	80
Jump delay	t_{delay} (μs)	500
Max. pulse energy	E (mJ)	0.4
Pulse repetition rate	PRR (kHz)	50
No. of passes	n	5
Focal position	f (mm)	0
Pitch	p (μm)	100
Positioning speed	v (mm/s)	5000
Machining rate	MR (cm^2/min)	2.03

TABLE 3 Laser Micromachining Parameters for Grid and Chaotic Surface Textures. Machining Conditions are Based on Linear Scanning

Parameter		Grid	Chaotic
Pulse energy	E (mJ)	0.5	0.5
Repetition rate	PRR (kHz)	50	50
No. of passes	n	50	5
Focal position	f (mm)	−0.6	0
Pitch	p (µm)	250	50
Scanning speed	v (mm/s)	100	150
Machining rate	MR (cm^2/min)	0.15	0.45

Further overlapping of the surface geometries would theoretically result in the complete machining of surface. However, with the opportune regulation of the process parameters, one can obtain a process that consists of both material removal and material movement. The last surface design, namely chaotic, derives from this fact, and incorporates all the features of the previous surfaces, as well as potentially providing undercuts (Fig. 1(c)). The moved and redeposited material creates micrometric free form structures that can be exploited for adhesion improvement. From this point of view, chaotic is a stochastic surface design obtained by the same principal processing used for direct writing. Laser micromachining of titanium and alloys with a pulsed nanosecond laser is known to generate layers of remelted material, which reduces the machining quality for most of the applications [26]. However, here it is used to move material and redeposit on the surface. For this purpose a short pitch was adopted at 50 µm, and with five consecutive passes the surface structure could be changed in the desired manner. The laser processing parameters for chaotic texture are shown in Table 3.

In addition to the geometrical differences, the designed surface textures differed in terms of productivity. A simple calculation can be derived to assess the productivity of applying the three different surface textures to a unit area.

For dimpling texture, which employs point-by-point percussion drilling strategy, the cycle time for a single microhole (t_m) is the sum of

$$t_m = t_{drill} + t_{delay} + t_{pos}, \tag{1}$$

where t_{drill} is the drilling, t_{pos} is positioning, and t_{delay} is the jump delay time, respectively. Drilling time is the used modulation duration (t_{mod}):

$$t_{drill} = t_{mod}. \tag{2}$$

The positioning time (t_{pos}) accounts for the time required to move the laser beam from one drilling point to the next. It depends on the scan speed (v) and the pitch (p) and can be simply expressed by

$$t_{pos} = \frac{p}{v}, \tag{3}$$

while jump delay (t_{delay}) is a constant value and is determined by the laser and scanner transitories. The sum of these three components (t_{mod}, t_{delay}, t_{pos}) have to be applied for the total number of microholes (D), by the number of passes (n), which gives the machining cycle time (t_{cycle}) as follows:

$$t_{cycle} = t_m \cdot D \cdot n. \tag{4}$$

The total number of microholes on a square surface texture with fixed pitch on both axes is given by the following equation:

$$D = \left(\frac{\sqrt{A}}{p} + 1 \right)^2, \tag{5}$$

where A is the surface area. In the end machining cycle (t_{cycle}) time becomes

$$t_{cycle} = \left(t_{mod} + t_{delay} + t_{pos} \right) \cdot D \cdot n. \tag{6}$$

Instead, for grid and chaotic textures, which employ linear scanning strategy, the machining cycle time is a function of total scanned distance. That is a function of the length of each scan (l) and the total number of scans (S) at each pass. On a square surface texture the length of each scan is equal to one side of the square area,

$$l = \sqrt{A}, \tag{7}$$

whereas the total number of scans depends on the number of lines on the other side of the square, distanced with the determined pitch (p). Since both horizontal and vertical lines are realized, the total number of scans becomes

$$S = \left(\frac{\sqrt{A}}{p} + 1 \right) \cdot 2. \tag{8}$$

Finally machining cycle time becomes the total scan length divided by the scan speed and can be calculated by the following expression:

$$t_{cycle} = \frac{S \cdot l \cdot n}{v}. \tag{9}$$

In the end, machining rate (MR) of each texturing methods can be expressed as the cycle time required to texture unit area as

$$MR = A / t_{cycle}. \tag{10}$$

In particular, on the present dimpling texture design with $p = 100\,\mu m$, inside a square shaped area with $A = 1\,cm^2$, $D = 10201$ microholes are present. With $v = 5000\,mm/s$ scan speed, the positioning time is calculated as $t_{pos} = 20\,\mu s$.

For $n=5$ passes, the calculated machining cycle time is $t_{cycle}=29.6$ s, thus the machining rate becomes $MR=2.03$ cm^2/min. For grid and chaotic texture types, the scan length in square area with $A=1$ cm^2 is $l=1$ cm. With $p=250$ μm the number of total scans for grid texture is calculated as $S=82$, whereas for chaotic texture with $p=50$ μm it is $S=402$. Accordingly for the given area, using respective scan speeds and number of passes the machining cycle times are calculated as $t_{cycle}=410$ s and $t_{cycle}=134$ s for grid and chaotic surface types, respectively. Corresponding machine rates are $MR=0.15$ cm^2/min for grid and 0.45 cm^2/min chaotic surface type. The analysis shows that the employed machining strategy not only defines the geometry, but also generates distinct productivity conditions. From this point of view, dimpling stands out as the most productive solution.

In order to compare the performance of the laser textured surfaces with a conventional method, sand blasted surfaces were also prepared. Sand blasting was applied with white corundum (mesh size 180) at 6 bar pressure according to the industrial practice. After sand blasting the specimens were cleaned with compressed air and washed in acetone.

2.2. Preparation of Adhesive Bonds

The textured pieces were bonded in a single lap joint configuration similar to that described by the ASTM-D1002-05 standard, in order to compare the apparent shear strength of the adhesively bonded metal specimens (Fig. 2) [27]. Deviations from the standard consisted of different specimen dimensions. Particularly, the adherents were cut out of 8 mm thickness plates and the specimens were overlapped in a region of 25.4 mm, where surface preparation and adhesive bonding were applied. Nevertheless, the tests allowed for comparison of results of the different surface treatments.

One essential factor for testing the adhesive strength of the metallic surfaces properly is to effectively separate them, in lap joint conditions. Bonding was designed so as to separate the Ti6Al4 V surfaces in order to evaluate just the titanium-adhesive adhesion and avoid interactions between the two plates. Also the adhesive has to penetrate the texture cavities to obtain a good bonding. A commercially available epoxy based adhesive from 3M^{TM} Scotch-Weld^{TM} DP 760 (Manchester, UK) was used. The adhesive was mixed
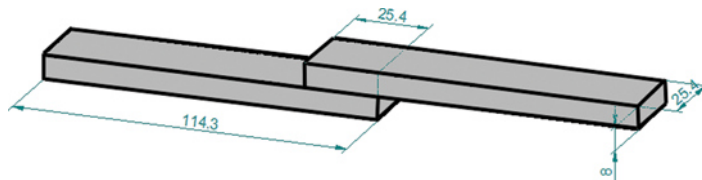
FIGURE 2 The shear test sample dimensions.

with 200 µm diameter glass spheres to separate surfaces of the two Ti6Al4V plates. The mixture contained 5 wt% of glass spheres. A cure cycle at 65°C and 100 kPa for 120 min was applied.

2.3. Characterization of Textured Surfaces and Bond Strength

The topography of the textured surfaces was characterized using two different methods: (i) scanning electron microscopy (Zeiss EVO-50 from Carl Zeiss, Oberkochen, Germany) to reveal the surface morphology; (ii) focus variation microscopy for 3D surface analysis and surface roughness evaluation (InfiniteFocus from Alicona Imaging GmbH, Graz, Austria). Same analyses were applied to sand blasted specimens for morphological comparisons. Surface chemistry was evaluated via energy-dispersive X-ray spectroscopy (EDS—7060 detector from Oxford Instruments, Oxford, UK) and X-ray diffractometry (XRD—X'Pert Pro from PANalytical, Almelo, the Netherlands). Surface wettability was estimated from digital images of distilled water droplets placed manually on the surface. Four CA measurements were taken on all specimens. Cross sections of the combinations of the different laser surface textures and adhesives were made and optical microscopy images were taken to evaluate cavity filling and specimen separation. The shear strength of the adhesion joints was measured using a hydraulic tensile testing machine (Landmark from MTS Eden Prairie, MN, USA) able to provide a maximum load of 100 kN. The tests were conducted at a crosshead speed of 1.3 mm/min and at room temperature. The strength of the laser textured joints was compared to the resistance of plain and sand blasted surfaces, since this process is common in the state of the art of adhesion enhancement. For every surface, the test was replicated twice in order to evaluate the repeatability of the processes.

3. RESULTS AND DISCUSSION

3.1. Morphological Analysis of Laser Textured Surfaces

Figures 3 and 4 report the SEM and focus variation microscopy images, respectively, of the sand blasted and laser textured surfaces. The sand blasted surfaces exhibit increased surface area due to increased surface roughness (Figs. 3(a) and 4(a)). On the other hand, laser textured surfaces show presence of recast material, a characteristic of the laser micromachining with ns-pulsed lasers. The recast material shows deviation from the conceptual design, which can induce benefits as well as drawbacks.

The generated dimpling texture was characterized by microholes 60 µm in diameter and 150 µm in depth. A portion of the removed material was re-deposited around the hole entrance, which is in the form of a crown (Fig. 3(b)). This portion of the recast introduces undercuts, and can be useful for mechanical interlocking of the adhesive to the surface. The rest of the
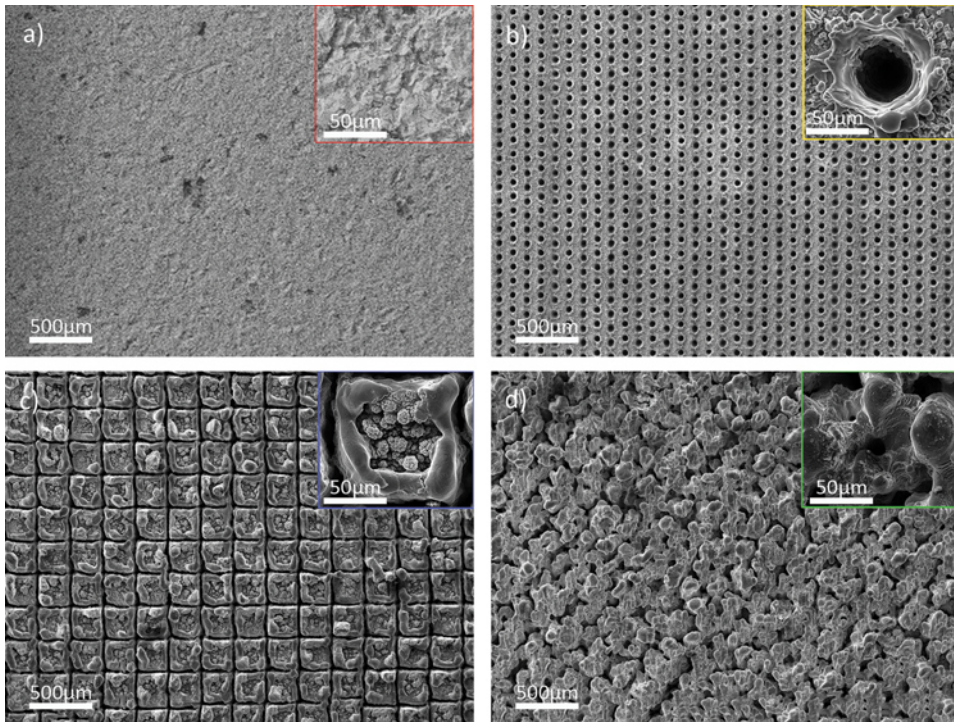
FIGURE 3 SEM images of the prepared Ti6Al4V surfaces: (a) sand blasted, (b) dimpling, (c) grid, and (d) chaotic.

recast is deposited between and inside the microholes. This can increase the overall surface roughness (Fig. 4(b)), which can cause changes in the wetting behavior. However, it should be noted that the adhesion of the recast layer to the bulk material can be lower than its adhesion to the adhesive.

The grid texture shows well-defined digs around the surface, as well as the recast layer that generates deviations from the intended geometry (Fig. 3(c)). Similar to dimpling, the recast generates undercuts over the surface which generates a closure on the singular square islands. Moreover the square islands show a fractal structure of recast layer, which may induce local differences in the surface wetting. In terms of characteristic measures, width is around 60 μm and the peak to valley depth of the digs is around 450 μm (Fig. 4(c)).

Figures 3(d) and 4(d) show the realized chaotic texture form. High surface roughness and a quasi-porous surface structure are the main characteristics of this surface type. Cracks generated due to the thermal process applied in ambient atmosphere can be seen in the high magnification inset of Fig. 3(d). Due to these factors the adhesion of the laser textured layer to the material bulk can be a critical factor. The peak to valley depth of the
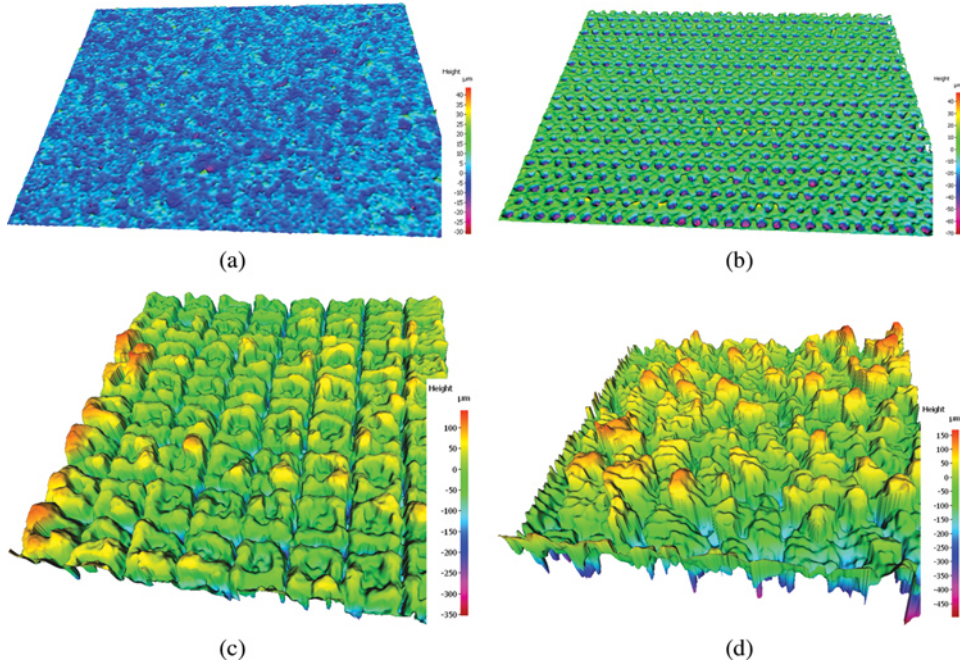
FIGURE 4 Focus variation microscopy images of prepared Ti6Al4V surfaces: (a) sand blasted, (b) dimpling, (c) grid, and (d) chaotic.

chaotic texture was about 250 μm, though a discontinuous depth profile was observed due to porous structure (Fig. 4(c)).

The focus variation microscopy images were also used to measure the surface roughness in terms of common parameters, average surface roughness R_a, root mean squared roughness R_q, and average distance between the highest peak and lowest valley R_z; although these parameters are not sufficient to describe the complex surface geometry, they are useful for a primary quantitative distinction between the surfaces. Five measurements taken on the same surface were used to calculate the confidence intervals of the measures. Figure 5 reports the measured surface roughness parameters belonging to different surfaces. As can be observed from Fig. 5, the sand blasted surfaces exhibit little change in average surface roughness compared to plain surfaces, as R_a values remain in the order of 1 μm, whereas the R_z value increases from 5 to 10 μm. The dimpling texture significantly increases the surface roughness due to the repeated surface microstructures. On the other hand, grid and chaotic textures show the highest surface roughness with very similar behavior. For grid and chaotic textures the large cavities generated on the surface increase the surface roughness mean values to around $R_a = 25$ μm, $R_q = 34$ μm, and $R_z = 130$ μm, with high variations in the measured ranges.
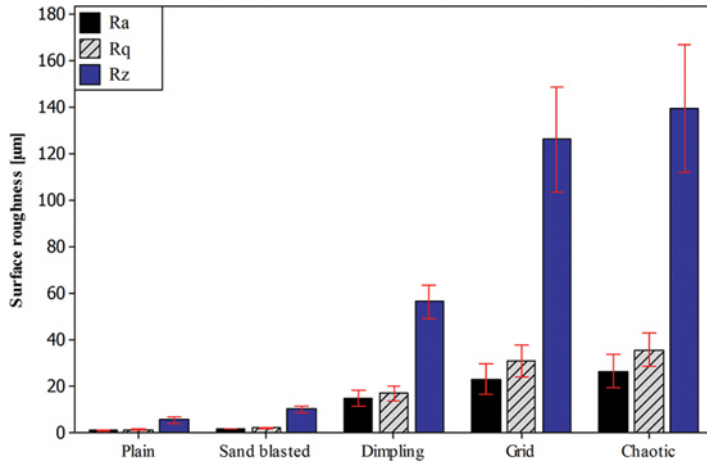
FIGURE 5 Surface roughness measurements belonging to different surface conditions, using different roughness indicators (error bars represent 95% confidence interval for the mean).

3.2. Characterization of Chemical Composition and Wettability of the Textured Surfaces

Table 4 shows the quantitative chemical compositions and generated oxide types on plain and laser surface textured samples. It can be seen that the higher energetic conditions are characterized by higher amount of oxygen percentage. Dimpling texture shows lowest amount of oxygen content (11 wt%) due to localized point-by-point processing and reduced number of passes. The grid and chaotic textures exhibited significantly increased oxygen content due to complete linear scans and higher pulse energy. The chaotic texture shows 26.8 wt% of oxygen, whereas the grid texture possesses the highest amount at 30.2 wt% due to increased number of passes. On the other hand in all cases, Al and V contents vary very little compared to the Ti content. This is a direct consequence of the high reactivity of Ti. The oxide types found on the textured surfaces are predominantly face-centered cubic (fcc) TiO and partially rutile TiO_2. Titanium reacts with oxygen to form amorphous TiO_2 initially. Amorphous TiO_2 can form anatase crystal form by annealing around 300°C. Above 700°C anatase TiO_2 converts to rutile crystal

TABLE 4 Chemical Composition, Oxide Types, and Estimated Contact Angles of the Plain and Laser Surface Textured Ti6Al4V Surfaces

Texture type	Ti wt%	Al wt%	V wt%	O wt%	Oxide type	CA
Plain	90.4	5.9	3.4	—	—	$44° \pm 8°$
Dimpling	80.5	4.9	3.5	11.1	Low amount of fcc TiO	$125° \pm 6°$
Grid	62.5	3.8	3.5	30.2	TiO_2 rutile > fcc TiO	$89° \pm 6°$
Chaotic	66.0	3.8	3.4	26.8	fcc TiO	$61° \pm 10°$

form. On the other hand non-stoichiometric TiO can be generated by direct reduction of Ti metal and TiO_2 mixture around 1600°C [28,29]. Generation of TiO from Ti targets via laser ablation in water has been reported previously [30,31]. Ablation in water permits the confinement of the plasma plume, which increases its pressure and temperature allowing TiO to be generated directly from Ti. In this work, it is observed that the processing conditions yielded surface temperature high enough to generate TiO on all textured surfaces. The XRD signals show weak presence of TiO on dimpled surface, which is coherent with the low oxide level found in the chemical composition analysis. The chaotic surface texture shows predominantly TiO on the surface, which is linked to the higher energetic condition. On the other hand the grid texture exhibits higher amount of rutile TiO_2 compared to TiO. As a matter of fact TiO reverts to TiO_2 on heating in air to 350°C. Thus, it is expected that due to increased number of passes applied in the strategy, an annealing effect is present, which reverts most of the TiO into rutile TiO_2.

The chemical state determines both mechanical and wetting performances of the surface texture. Oxides of titanium are ceramics, therefore are characterized by increased brittleness compared to the Ti metal. Flat rutile surfaces exhibit CAs around 80° [32]. On the other hand, the wettability of flat TiO surfaces is not present in the literature. The estimated CAs show that the plain Ti6Al4 V surface is moderately hydrophilic ($CA = 44° \pm 8°$). On the other hand chaotic and grid surface textures show increased CAs, $61° \pm 10°$ and $89° \pm 6°$, respectively. An ideally flat hydrophilic surface should reduce CA with the increase of the surface area as expressed by the Wenzel equation [33]:

$$\cos \theta_r = r \cos \theta_f, \tag{11}$$

where θ_f is the CA of flat surface and θ_r is the CA of rough surface as with $r > 1$. Both grid and chaotic surface texture types show increased surface area, therefore the increase in the CA should be associated to the change of surface chemistry. On the other hand the dimpling surface texture shows highly hydrophobic behavior ($CA = 125° \pm 6°$). Such high CA value is attributed to air entrapment in the blind microholes.

3.3. Characterization of the Adhesive Bond Cross Sections

Figure 6 reports the cross sections of the adhesive bonds with different surface texture types. In the case of dimpling, it is noticed that complete filling of the microholes could not be achieved. This is attributed to the fact that the microholes generate air entrapment and increased capillary pressures that is required to exert the adhesive in order to fill the cavity completely. Grid and chaotic textures do not present filling problems, and moreover complete separation of the plates was satisfied when glass spheres were used. The minimum distance between the plates was measured to be higher than
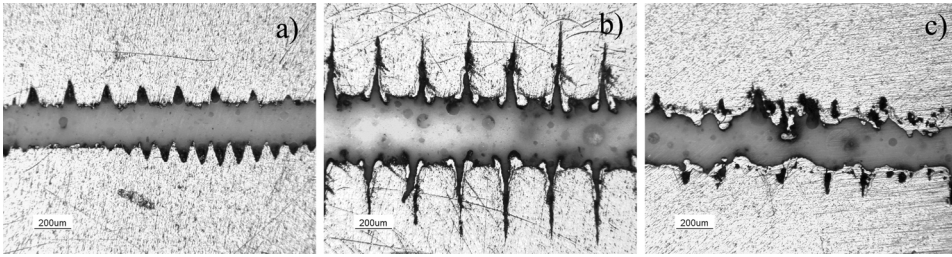
FIGURE 6 Cross sections belonging to different adhesive bonds on (a) dimpling, (b) grid, and (c) chaotic surface textures, depicting filling of the generated cavities, and separation of the opposite Ti6Al4V plates.

200 µm in all cases, which ensures that the gap is larger than the glass spheres and they are not in contact at least with both of the surfaces at the same time.

3.4. Characterization of the Bonding Strength

The results of the apparent shear tests referring to different surfaces are shown in Fig. 7. Tensile tests on single lap joints allow the apparent shear strength to be evaluated defined as the maximum force value reached during the tests
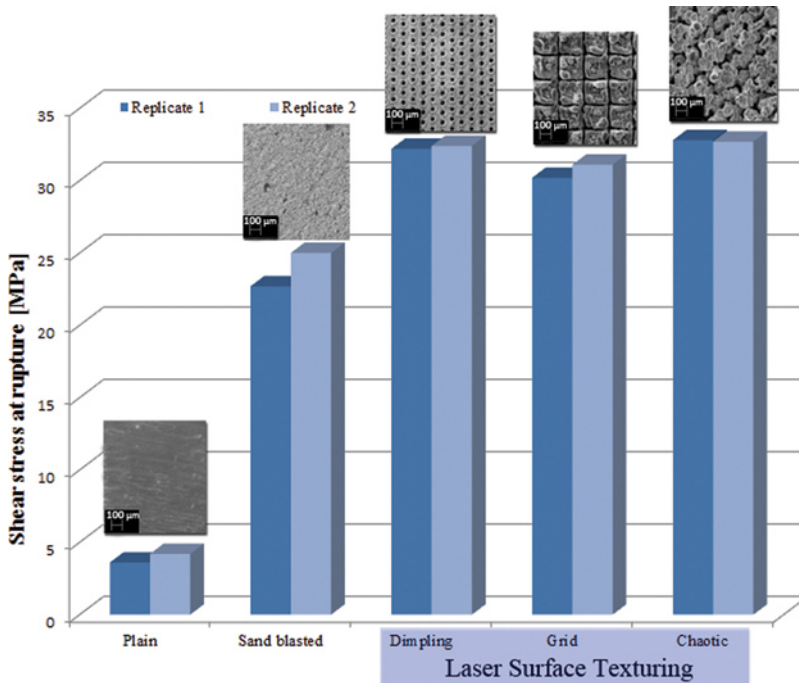
FIGURE 7 Adhesive bonding performance of plain, sand blasted, and laser surface textured surfaces as a function of shear stress at rupture. The graph shows two replications for each condition.

divided by the overlap area. This value differs from the maximum local shear stress. In fact, the actual shear stress distribution along the bond-line is non-uniform and displays two symmetric peaks at the overlap ends. Moreover, due to the rotation of the joint during the test, normal stresses are also present. However, the apparent shear strength is a useful parameter for comparison purposes (if nonlinear effects are absent, as in the case of thick titanium adherents, the peak stresses at failure are proportional to the apparent shear strength). The non-treated Ti6Al4V specimens exhibit bond failure when reaching apparent shear strength of 3.9 MPa. Compared to plain surfaces, all treated surfaces show increased adhesion strength. Sand blasted specimens failed at 23.4 MPa, which is the case that showed the highest variance in the shear strength. This can be attributed to the low controllability of the obtained surface texture by this process. On the other hand, all types of laser textured surfaces show better performance compared to plain and sand blasted surfaces. Similar apparent shear stress values are observed, as grid, dimpling, and chaotic failed at 30.7, 32.3, and 32.8 MPa, respectively. These measures show that laser surface texturing improve the adhesion strength of up to eight times the resistance of a plain surface, and up to 37% more than a sand blasted surface with reduced variability in the bond strength. However, these values do not show any significant difference between different surface textures. Therefore, a fracture analysis is suitable to determine the mechanism of failure.

4. FAILURE ANALYSIS

Fracture surfaces were observed using at different magnifications the same SEM equipment described in Section 1.3. Images of the fracture surface of the sand blasted, dimpling, grid, and chaotic cases are shown in Fig. 8. From the observation of the fracture surface of one sand blasted specimen it appears clearly that it underwent adhesive failure. In the case of the specimen belonging to the dimpling category, a mixed behavior was observed, with a large portion of the fracture surface showing signs of adhesive failure. It also appears clearly that most of the dimples did not retain any trace of adhesive. However, apparent shear strength values suggest that laser texturing allowed for enhancing the adhesion strength, as compared with the sand blasted surface.

A more pronounced effect of the surface texturing on the extension of the cohesive surface area can be observed in the case of the grid pattern. In this case, the majority of the fracture surface appears as cohesive. In the case of the chaotic pattern, a different behavior was observed, characterized by the failure of the adherent's surface, as witnessed by a thin layer of metal debris still adhering on the mating surface. Although comparison of the apparent shear strength values suggest that an equal effect on mechanical performances was obtained by all the laser texturing methods, the observed differences in the failure surface aspect indicate that the grid pattern is likely
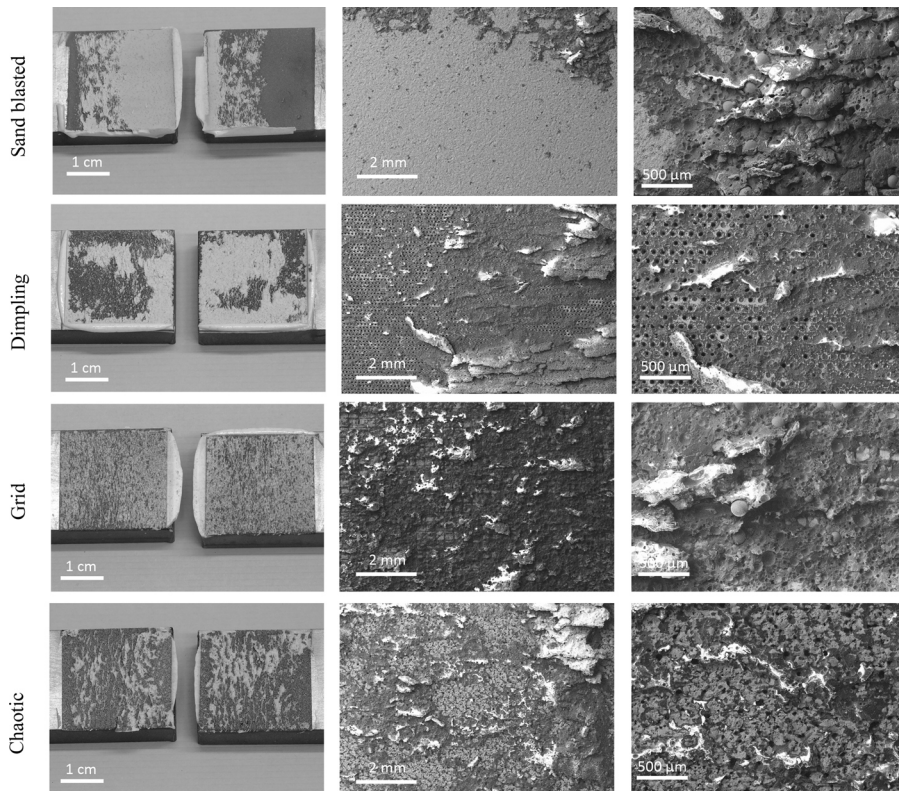
FIGURE 8 Macro-photographs of the tested Ti6Al4V plate pairs and SEM images of the surfaces after shear tests, depicting the conditions of the adhesive and the treated surface.

to have allowed for the best mechanical interlocking effect. For both grid and chaotic surface textures poor wettability indicated by the measured CA values ($CA = 61\text{–}89°$) appears to be overcome by the applied pressure during the adhesive bonding phase, allowing better filling of the texture cavities and generating the required mechanic interlock. The chaotic pattern is likely to have weakened the surface, either by creating brittle oxides or severe undercuts. In the case of the dimpling pattern, the adhesive could not flow into the microholes. This is coherent with the hydrophobic behavior observed in the wettability measurements ($CA = 125°$). Apparently, the applied pressure was not sufficient to exert the adhesive into cavities and mechanical interlocking was not fully provided. This fact suggests that the depth of the holes could have been reduced without affecting the surface strength.

5. CONCLUSIONS

This work reports the results of preliminary investigations on the use of laser surface texturing to improve the adhesive bonding of Ti6Al4 V alloy. The

study explored three distinct surface textures, with the aim to reveal the potentiality of such processing method as an alternative to other surface treatments and as an environmentally friendly surface preparation method, compared to treatments involving hazardous chemicals. The conceptualized surface textures were realized with different laser micromachining strategies that involved point-by-point microdrilling and surface scanning. The resultant surfaces deviated from the ideal ones mainly due to the generation of molten material. The shear tests were applied on the plain, sand blasted, and laser textured surfaces for comparison of adhesive bond strength. All laser textured surfaces showed significant improvement in maximum apparent shear stress compared to the sand blasted surfaces. Although the maximum shear strength of the different texture types did not differ significantly, they showed distinct failure mechanisms: partial cohesive failure for dimpling, fully cohesive failure for the grid pattern, and failure of the textured substrate in the case of the chaotic pattern.

Although these results do not cover all possible surface treatments solutions, they indicate that the use of laser textured surfaces constitute a viable option to improve adhesion joint strength. Two directions emerge for future works regarding improving productivity and optimizing surface geometry for increased adhesive bonding performance. From the highest productivity point of view the dimpling strategy appears to be more convenient. The productivity can be further increased by reducing the applied number of passes to achieve shallower holes. As a matter of fact the filling of deeper cavities becomes more difficult and the reduction of the hole depth is not expected to degrade the adhesive bond performance. On the other hand, grid strategy shows higher potential to improve the bonding performance, given the fact that the specimens showed a cohesive failure mechanism in the experimentation. Future works will be dedicated to study the key parameters of the surface groove depth, width, and pitch to optimize adhesive bond strength. The performance of the chaotic surface texture can be improved via processing in inert atmosphere. However, the porous structure and the adhesion of the textured surface to the bulk material constitute the greater limitations regarding possible improvements.

REFERENCES

[1] Ezugwu, E. O. and Wang, Z. M., *J. Mater. Process. Technol.* **68**, 262–274 (1997).

[2] Ezugwu, E. O., Bonney, J., and Yamane, Y., *J. Mater. Process. Technol.* **68**, 262–274 (1997).

[3] Barreda, J. L., Santamaria, F., Azpiroz, X, Irisarri, A. M., and Varona, J. M., *Vacuum* **62**, 143–150 (2001).

[4] Li, Z., Gobbi, S. L., Norris, I., Zolotovsky, S., and Richter, K. H., *J. Mater. Process. Technol.* **65**, 203–208 (1997).

[5] Zhang, Y., Sato, Y. S., Kokawa, H., Park, S. H. C., and Hirano, S., *Mater. Sci. Eng., A* **485**, 448–455 (2008).

[6] Molitor, P. and Young, T., *Int. J. Adhes. Adhes.* **22**, 101–107 (2002).

[7] Bhowmik, S., Bonin, H. W., Bui, V. T., and Weir, R. D., *Int. J. Adhes. Adhes.* **26**, 400–405 (2006).

[8] Bhowmik, S., Benedictus, R., Poulis, J. A., Bonin, H. W., and Bui, V. T., *Int. J. Adhes. Adhes.* **29**, 259–267 (2009).

[9] Cognard, P., *Handbook of Adhesives and Sealants, Volume 1: Basic Concepts and High Tech Bonding*, (Elsevier Science, Versailles, 2005). Chap. 4, pp. 196–202.

[10] Critchlow, G. W. and Brewis, D. M., *Int. J. Adhes. Adhes.* **15**, 161–172 (1995).

[11] Higgins, A., *Int. J. Adhes. Adhes* **20**, 367–376 (2000).

[12] Molitor, P., Barron, V., and Young, T., *Int. J. Adhes. Adhes.* **21**, 129–136 (2001).

[13] Baldan, A., *J. Mater. Sci.* **39**, 1–49 (2004).

[14] Mertens, T., Gammel, F.J., Kolb, M., Rohr, O., Kotte, L., Tschoecke, S., Kaskel, S., and Krupp, U., *Int. J. Adhes. Adhes.* **34**, 46–54 (2012).

[15] Galantucci, L. M., Gravina, A., Chita, G., and Cinquepalmi, M., *Composites Part A* **27A**, 1041–1049 (1996).

[16] Wong, R. C. P., Hoult, A. P., Kim, J. K., and Yu, T. X., *J. Mater. Process. Technol.* **63**, 579–584 (1997).

[17] Molitor, P. and Young, T., *Int. J. Adhes. Adhes.* **24**, 127–134 (2004).

[18] Baburaj, E. G., Starikovb, D., Evans, J., Shafeev, G. A., and Bensaoula, A., *Int. J. Adhes. Adhes.* **27**, 268–276 (2007).

[19] Spadaro, C., Sunseri, C., and Dispenza, C., *Radiat. Phys. Chem.* **76**, 1441–1446 (2007).

[20] Man, H. C., Chiu, K. Y., and Guo, X., *Appl. Surf. Sci.* **256**, 3166–3169 (2010).

[21] Lamraoui, A., Costil, S., Langlade, C., and Coddet, C., *Surf. Coat. Technol.* **205**, S164–S167 (2010).

[22] Çelen, S., Efeoğlu, C., and Özden, H., *Phys. Procedia* **12**, 245–251 (2011).

[23] Man, H. C., Wang, Q., and Guo, X., *Opt. Laser Eng.* **48**, 583–588 (2010).

[24] Alfano, M., Pini, S., Chiodo, G., Barberio, M., Pirondi, A., Fugiuele, F., and Groppetti, R., *J. Adhes.* **90**, 1–16 (2014).

[25] Demir, A. G., Previtali, B., and Lecis, N., *Opt. Laser Technol.* **54**, 53–61 (2013).

[26] Demir, A. G., Previtali, B., and Bestetti, M., *Physics Procedia* **5**, 317–326 (2010).

[27] ASTM-D1002-05 Standard Test Method for Apparent Shear Strength of Single-Lap-Joint Adhesively Bonded Metal Specimens by Tension Loading (Metal-to-Metal).

[28] Cardarelli, F., *Materials Handbook: A Concise Desktop Reference*, (Springer, London, 2000).

[29] Neupane, M. P., Park, I. L., Leeb, M. H., Bae, T. S., and Watari, F., *Biomed. Mater. Eng.* **19**, 77–83 (2009).

[30] Semaltianos, N. G., Logothetidis, S., Frangis, N., Tsiaoussis, I., Perrie, W., Dearden, G., and Watkins, K. G., *Chem. Phys. Lett.* **496**, 113–116 (2010).

[31] Huang, C. N., Bow, J.-S., Zheng, Y., Chen, S. Y., Ho, N. J., and Shen, P., *Nanoscale Res. Lett.* **5**, 972–985 (2010).

[32] Hashimoto, K., Irie, H., and Fujishima, A., *Japan. J. Appl. Phys.* **44**, 8269–8285 (2005).

[33] Wenzel, R. N., *Ind. Eng. Chem.* **28**, 988 (1936).